A fresh look at dense hydrogen under pressure. II. Chemical and physical models aiding our understanding of evolving H–H separations

Vanessa Labet, Roald Hoffmann, and N. W. Ashcroft

Additional information on J. Chem. Phys.

A fresh look at dense hydrogen under pressure. II. Chemical and physical models aiding our understanding of evolving H–H separations

Vanessa Labet,[1,a)] Roald Hoffmann,[1,b)] and N. W. Ashcroft[2]

[1]*Department of Chemistry and Chemical Biology, Cornell University, Baker Laboratory, Ithaca, New York 14853, USA*
[2]*Laboratory of Atomic and Solid State Physics and Cornell Center for Materials Research, Cornell University, Clark Hall, Ithaca, New York 14853, USA*

In order to explain the intricate dance of intramolecular (intra-proton-pair) H–H separations observed in a numerical laboratory of calculationally preferred static hydrogen structures under pressure, we examine two effects through discrete molecular models. The first effect, we call it physical, is of simple confinement. We review a salient model already in the literature, that of LeSar and Herschbach, of a hydrogen molecule in a spheroidal cavity. As a complement, we also study a hydrogen molecule confined along a line between two helium atoms. As the size of the cavity/confining distance decreases (a surrogate for increasing pressure), in both models the equilibrium proton separation decreases and the force constant of the stretching vibration increases. The second effect, which is an orbital or chemical factor, emerges from the electronic structure of the known molecular transition metal complexes of dihydrogen. In these the H–H bond is significantly elongated (and the vibron much decreased in frequency) as a result of depopulation of the σ_g bonding molecular orbital of H_2, and population of the antibonding σ_u^* MO. The general phenomenon, long known in chemistry, is analyzed through a specific molecular model of three hydrogen molecules interacting in a ring, a motif found in some candidate structures for dense hydrogen. © *2012 American Institute of Physics.* [http://dx.doi.org/10.1063/1.3679736]

I. INTRODUCTION

A. Reminder

In the preceding paper,[1] we examined the evolution of the shortest and second shortest proton-proton separations in those structures predicted by Pickard and Needs[2] to be the most stable arrangements for solid hydrogen under pressure. The first corresponds to the proton-proton separations within H_2 units and the second corresponds to the shortest proton-proton separations between neighboring H_2 units. As in the preceding paper, and with full awareness of the limitations of using molecular language at high hydrogen densities, we will refer to these in the following as the intramolecular and shortest intermolecular H–H separations, respectively.

The theoretically determined static structures serve as a kind of structural laboratory for learning more about hydrogen under pressure. By following the most stable structure of solid hydrogen between 1 atm and 500 GPa, the shortest intermolecular H–H separation has been seen to decrease with pressure, whereas the intramolecular counterpart, while changing little in an absolute sense, at first decreases, then increases, but yet again decreases. We introduced in the first paper[1] a convenient measure of this behavior, an equalization function $\xi(P)$, which takes on values between 0 and 1. Assuming that the structures studied are reasonable (and there are

experimental points of contact that provide confirmation that we will come to below), hydrogen enters a metallic state while the degree of equalization of the intramolecular and shortest intermolecular H–H separations remains only ∼90%. In other words, hydrogen seems to resist perfect equalization of its H–H distances even as it metallizes.

The aim of the present paper is to present discrete models which will assist in delineating the physical and chemical mechanisms at work in altering the H–H separations as pressure is applied, and thereby to hone our understanding of the role of the different regimes of local density which affect the intramolecular H–H separations.

B. Experimental information

Experimentally, the evolution with pressure in solid hydrogen of the intramolecular H–H distances—or the H–H bond length of the H_2 units—and their associated binding has been followed spectroscopically, rather than by x-ray diffraction (the scattering from H being weak). The roton, libron, and vibron frequencies are relatively easy to observe. The vibron frequency of a H_2 molecule, whether isolated or in a solid, is related to, to use a *classical* term, the H–H force constant, whereas the roton frequency gives us mainly the moment of inertia of the molecule and from it the H–H separation. The frequencies of the roton modes are much lower than those of the vibrons (by about a factor of 10), and the associated relative displacements can be quite substantial.

The link between bond length and bond strength (a longer bond corresponding to a weaker bond) is known as Badger's

---

a)Present address: LADIR (UMR 7075 CNRS/UPMC), Université Pierre et Marie Curie, 4 Place Jussieu, 75252 Paris Cedex 05, France.
b)Author to whom correspondence should be addressed. Electronic mail: rh34@cornell.edu.

rule,[3–5] and has long been a part of chemistry and physics, even as exceptions are well known.[6] A theory of the manner in which the intermolecular forces affect the infrared and Raman spectra of the solid compared to those of a free H_2 molecule in a gas was developed by Van Kranendonk.[7–10] The analysis by Loubeyre *et al.*[11] and Grazzi *et al.*[12] of the roton bands measured by Silvera and Wijngaarden[13] in *para*-H_2 at T = 6 K indicates that the intramolecular H–H separation decreases as P rises from 1 atm to 30 GPa, but thereafter increases. And the Raman spectra of solid *normal* H_2 recorded by Sharma *et al.*[14,15] at T = 298 K also contain indications of intramolecular H–H stiffening from 5.5 GPa (the pressure of solidification at T = 295 K) to 36 GPa ($r_s = 1.74$), followed by weakening with increased pressure.

II. METHODS AND COMPUTATIONAL DETAILS

The discrete molecular systems studied here were modeled using the GAUSSIAN 03 package.[16] Given a statement of the nuclei involved, the total number of electrons in the system, and a trial starting geometry, the optimal geometries were computed within the Born-Oppenheimer framework, using methods based either on the Møller-Plesset perturbation theory,[17] with corrections at the second-order,[18–21] or with the density functional theory,[22] using the B3LYP hybrid functional.[23–25] In each case, a triple-zeta basis set, with additional diffuse and polarization functions (6-311++G(d,p)), has been used. The optimizations were performed under geometrical constraints used to reflect the effect of pressure. Further details will be given later on the actual constraints chosen. For the last model we present Mulliken overlap population (MOP), Mayer bond order (MBO), and natural bond orbital (NBO) (Ref. 26) population analyses, performed to study the evolution of intramolecular and intermolecular H–H bonding.

III. TWO COMPETING EFFECTS INFLUENCING THE H_2 BOND LENGTH

As mentioned previously, both experimental measurements[11,13] and theoretical modeling[1] suggest that under pressure (and while passing through several distinct phases) the evolution of the intramolecular H–H separation in solid hydrogen proceeds through three main regimes: In the first (below P = 30–40 GPa according to the experimental evidence—and shifted to higher pressure (∼100 GPa) in our theoretical modeling), the H–H bond is shortened and, in agreement with Badger's rule, stiffened; in a second regime it is lengthened and also weakened, but only to later shorten further in a third regime at still higher pressures. We now turn to an explanation of these experimental and theoretical observations, using a sequence of numerical experiments performed on discrete models for the molecules in solid hydrogen.

A. Shortening and stiffening of the intramolecular H–H bond at low pressures

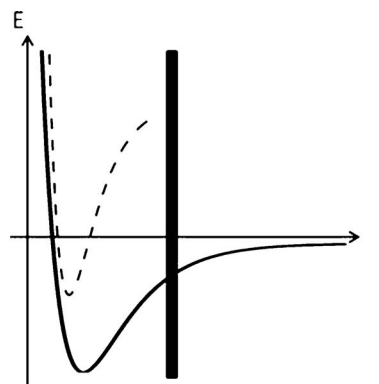Consider now what happens to a normal diatomic potential energy curve, E(r), (Fig. 1, solid line) as other molecules

FIG. 1. Schematic representation of the "physical wall" (black vertical bar) for nuclear motion formed around a diatomic molecule by surrounding molecules under increase in pressure. The solid black line represents the potential energy curve for an isolated diatomic molecule and the dashed line that of a diatomic molecule experiencing the presence of other molecules in its neighborhood.

begin to invade the neighborhood of a chosen molecule. Because of Pauli repulsion, it is very unfavorable for two molecules to be too close to each other and they will tend to resist such a merger. A molecule's extension is thus expected to be constrained by other neighboring molecules as pressure increases.

The thick vertical bar at the right in Fig. 1 is a symbolic "pressure wall" originating with the presence of surrounding and encroaching molecules. Note that by reciprocity, the diatomic molecule whose potential energy curve is plotted in Fig. 1 constrains in its turn the extension of surrounding molecules. The "pressure wall" will affect the molecule most on the dissociative, low energy side of E(r) (Fig. 1). Large intramolecular separations at fixed density are thus expected to be subject to an energy penalty. The result is that under pressure a new effective E′(r) results (the dashed line). Clearly E′(r) will have a shorter equilibrium separation, and a higher "force constant" in the harmonic approximation than will E(r).

1. A molecule in a spheroidal box

The effect of the "physical wall" described qualitatively above on the vibrational properties of H_2 molecules has been investigated computationally by LeSar and Herschbach in 1981.[27] They considered one H_2 molecule and defined a confining spheroidal boundary around it, placing the two protons at its foci, as sketched in Fig. 2.

The bounding region was made rigid by imposing an infinite potential outside of it. The effect of pressure was then modeled by varying the semimajor axis length $\frac{1}{2} R\lambda_0$ ($\lambda_0 > 1$) of the spheroidal region. For several imposed values of the semimajor axis length, the optimal value of the intramolecular H–H separation—R—was computed (and thus the optimal eccentricity $1/\lambda_0$ of the spheroid), by a variational calculation, employing a James-Coolidge wave function.[28] The total energy curves that were obtained for the protons are reproduced in Fig. 3.
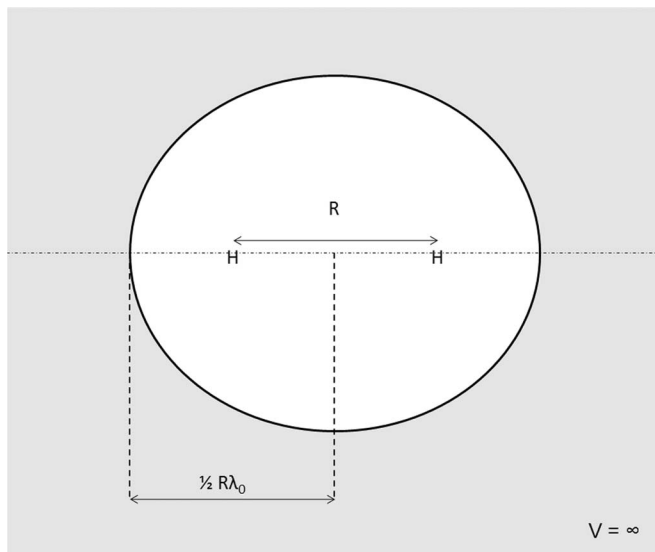
FIG. 2. H_2 molecule confined within a rigid prolate spheroidal boundary. The parameter λ_0 is related to the eccentricity of the spheroid. Protons reside at H and H.

As the size of the constraining spheroid decreases (i.e., as the length of the semimajor axis decreases), the optimal H–H separation of the H_2 molecule shortens. Because for decreasing size, the constraint exerted on the H_2 molecule is more and

more severe, the energy curve globally increases in energy. Below a certain volume of the boundary region, the minimum of the energy curve for the protons arising from the optimal electron density of two electrons becomes even higher in energy than that of two unconstrained protons at infinite separation. Nonetheless, there is still a clear preference for a distinct H–H separation, implying the existence of a H–H bond. In fact, the shape of the wells clearly shows that as the size of the boundary region decreases, the H–H bond shortening is correlated with a stiffening of the bond, this also reflected in the effective spring constant k.

2. A molecule in a softer box

The same trend observed by LeSar and Herschbach can also be obtained by constructing a "molecular physical wall," which, unlike the previous example, can exhibit a varying degree of softness. As a specific example, consider the following very simple model: two helium atoms surround a pair of H atoms, all on a line as sketched in Fig. 4. The heliums provide the requisite Pauli repulsion, but are "softer" than the rigid wall introduced above.

To simulate an increase in pressure, we fix the distance d between the outer He atoms and the center of the pair of H atoms at four different values: 3.0 Å, 2.0 Å, 1.5 Å, and 1.0 Å. We then optimize under the constraint of a fixed distance d the H–H separation $r_{H–H}$. Then, for each d, we perform single point calculations scanning the $r_{H–H}$ distance around its optimal value r_{eq}. The computations here were carried out at the level of the Møller-Plesset perturbation theory[17] with corrections at the second-order[18] (MP2/6-311++G(d,p)). The energy curves obtained are plotted in Fig. 5.

From the resulting curves were extracted (i) the optimal H–H separation (r_{eq}), and (ii) its equivalent force constant (k), by fitting the lower region of the wells by a quadratic function of the form $E - E_{eq} = \frac{1}{2}k(r_{H–H} - r_{eq})^2$. The results are given in Table I.

As expected, the smaller is r_{eq}, the larger is k. In other words, the shorter the H–H bond, the stiffer is the spring describing that bond. We might mention here that we tested the implicit Badger relationship between k and r_{eq} (as detailed in Ref. 3) and found that it was quite well satisfied in this model.

Our first thought was that He atoms would not interact significantly with the H_2. At extreme pressure (here modeled by a small d distance) in fact we do observe some electron transfer at low d from the atomic $1s$ orbitals of the He atoms
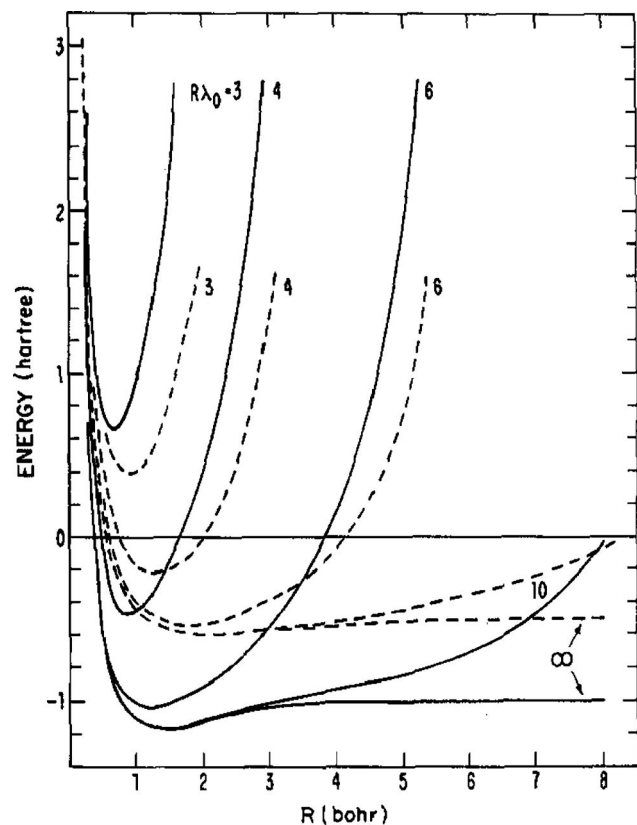

FIG. 3. Energy curves for the protons of a H_2 molecule (solid curves) and of a H_2^+ molecular ion (dashed curves) in spheroidal bounding regions of different sizes as characterized by their major axis lengths $R\lambda_0$, with respect to the internuclear distance R. Note that the distances are expressed in Bohrs. As $R\lambda_0 \rightarrow +\infty$, the spheroidal box becomes spherical. Reprinted with permission from R. LeSar and D. R. Herschbach, J. Phys. Chem. **85**, 2798 (1981). Copyright 1981 American Chemical Society.
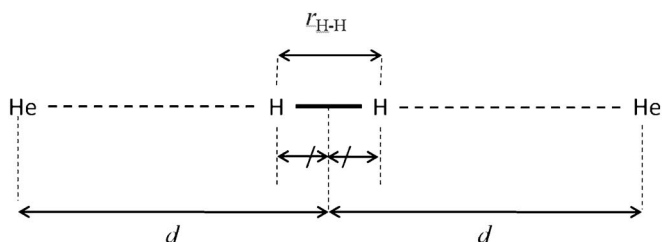

FIG. 4. Two He atoms surround a H atom pair in a collinear arrangement: a primitive molecular model considered in studying the shortening of the H_2 bond length under pressure.
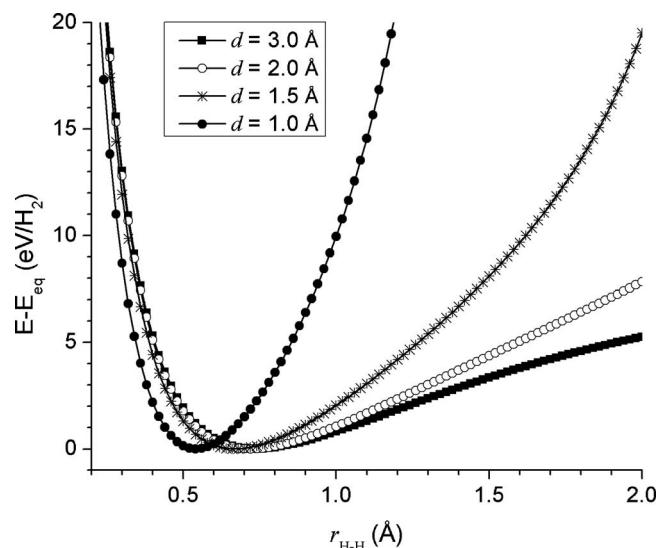
FIG. 5. Computed energy curves associated with the elongation of the central H–H entity of the system sketched in Fig. 4, keeping the two helium atoms fixed, under the constraints d = 3.0 Å (filled squares), 2.0 Å (empty circles), 1.5 Å (crosses), and 1.0 Å (filled circles) (see Fig. 4 for the definition of d). In each case, the potential energy for the protons is expressed as an energy relative to the energy at the constrained equilibrium (E_{eq}).

into the σ_u*, formally unfilled molecular orbital of the H_2 molecule. But this is anticipating Sec. III B.

Let us summarize what we learn from those two numerical experiments—one in the literature, one our own. Strict spatial confinement of a H_2 molecule—in a nuclear and electronic sense—tends to shorten and stiffen the H–H bond relative to that of a free H_2 molecule. As the size of the constraining region decreases, both the H–H shortening and concomitant stiffening rise in scale. Similar effects are observed in the case of "softer" spatial confinement arising from the presence of rather inert chemical species in the vicinity. This invasion by neighboring molecules is a natural consequence of pressure increase in molecular solids. We believe that soft molecular spatial confinement is at work in solid hydrogen in the pressure regime 1 atm to 30 GPa where the intramolecular H–H separation shortens and the interaction stiffens as the pressure increases. This is recorded in the experiments by the increase of both the vibron (higher bond force constant leading to a higher energy vibron) and also the roton frequencies under pressure.

TABLE I. Optimal values for r_{H-H} under a constraint of fixed d, and related force constant k of the central H–H pair deduced from a fit of the lower region of the wells plotted in Fig. 5 by a quadratic function.

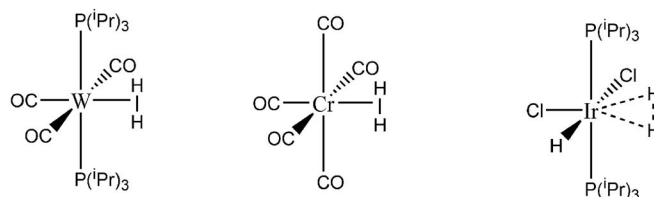| d (Å)	$r_{H-H,eq}$ (Å)	k (eV Å^{-2})
3.0	0.7377	40.6
2.0	0.7194	47.0
1.5	0.6680	63.0
1.0	0.5422	150.8

FIG. 6. Three examples of side-on bonded di-hydrogen complexes. Here, ^{i}Pr stands for iso-propyl (–CH–(CH$_3$)$_2$); CO for carbon monoxide. Plain lines indicate relatively strong bonds between the transition element center and the atoms/groups of atoms to which it is bonded (ligands). Dashed lines indicate weaker bonds.

B. Lengthening and softening of the intramolecular H–H bond at higher pressures

1. Side-on bonded H_2 molecules in organometallic complexes: An important "molecular" interlude

Because of their connections to the dense hydrogen problem it is time to introduce here a group of known discrete molecules in which an intact but strongly perturbed H_2 molecule (or several) is (are) bonded to a transition element center M, but in such a way that the H–H bond of the H_2 molecule is actually perpendicular to the M–(H$_2$) bond (see Fig. 6).[29–31] They are called η^2 or *side-on* bonded dihydrogen complexes. To look at these is not a digression at all; the behavior of these systems is useful in contemplating the emerging behavior in pure hydrogen itself under pressure.

The first of these complexes to be prepared and characterized was [W(CO)$_3$(P^{i}Pr)$_2$(H$_2$)], in a study by Kubas in 1984.[32] In the same year, an independent analysis by Saillard *et al.* laid the theoretical foundation for an understanding of their electronic structure.[33] Since then, several hundred H_2 complexes have been synthesized. Some selected structures are shown in Fig. 6.

The H–H distance in these has in some cases been quite accurately determined from neutron diffraction and also solid-state NMR measurements. The H–H separation is typically 0.82–0.89 Å—which is 10%–20% longer than in an isolated H_2 molecule—with less elongation in weakly bonded species such as Cr(CO)$_5$(H$_2$) (available only as matrix isolated species)[34] and with a more perturbed, longer H_2 separation in a few instances such as ReH$_5$(H$_2$){P(p-tolyl)$_3$}$_2$.[35] The H_2 vibron in these molecules is also perturbed far more than in the range of high pressure studies we discussed above—in fact, it is often as low as $\sim$3000 cm^{-1} (in an isolated H_2 molecule it is 4161 cm^{-1}).

The characteristics of the bonding in these side-on bonded dihydrogen complexes are sketched out in Fig. 7: if one considers an octahedral complex of ML$_5$(H$_2$) formula where L is a generic notation to designate an atom or a group of atoms bonded to M (a ligand), the nature of the bonding between M and H_2 can be deduced from the interaction between the ML$_5$ and H_2 fragments. There is electron donation from the ML$_5$ fragment into H_2 σ_u*, acceptance by an ML$_n$ orbital from H_2 σ_g, both lengthening the H–H bond relative to the separation in the free H_2 molecule.

Although there is no question that the side-on mode of coordination of the H_2 unit to the transition metal element
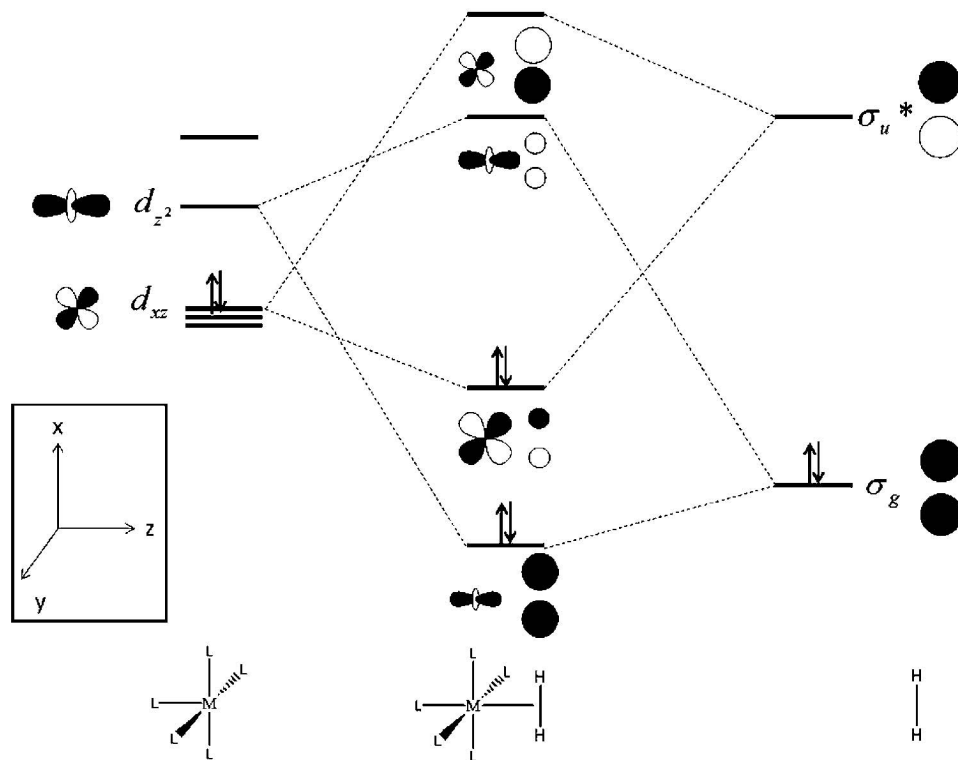
FIG. 7. A general molecular orbital (MO) interaction diagram for $ML_5(H_2)$ octahedral complexes constructed from an ML_5 and a H_2 fragment (adapted from Ref. [33]). Here, M is a generic transition element atom, L is an associated ligand, σ_g and σ_u^* are the bonding and antibonding H_2 molecular orbitals. Black and white indicate phases (and their differences) of the wave functions; no implications are being inferred of the coefficient amplitudes. The dashed lines simply indicate the presence of significant interactions.

M finds its origin in the orbital interactions highlighted in Fig. 7, it should be noted that the anisotropy of the dipole-polarizability also favors this side-on arrangement. At longer distances between the H_2 molecule and the transition metal element, now out of the range of substantial overlap between the orbitals of each of the ML_5 and H_2 fragments, this contribution is likely to govern their relative orientation; at the anticipated short separations of both the molecular complex and hydrogen under some pressure, this electrostatic factor is not likely to be important.

2. The chemical or orbital model for bond elongation in hydrogen under pressure

The bonding model of Fig. 7 for a metal fragment with its associated ligands, interacting with a H_2 molecule, is in fact closely related to what is happening when two H_2 molecules—let us call them A and B—are forced to interact at high pressure, provided that the bandwidths induced by intermolecular interactions are themselves small compared to the bandgap. In the study by Pickard and Needs,[2] among the four molecular structures considered, only the *Cmca* structure,[36] which is the most stable from P = 385 GPa to P = 490 GPa, is metallic within its range of stability. While retaining pairing, it is estimated to metallize by band overlap around P = 410 GPa.[2,36,37] Over most of the pressure range we explore here orbital interactions are likely to give a good qualitative description of the development of the electronic structure. The progression of the analysis is indicated in

Fig. 8. As the interaction between the two H_2 molecules A and B takes place, the mutual interactions between electrons and nucleus of A and also those of B can be treated as a perturbation of the interactions already involved in molecules A and B, separately.

First, at the left of Fig. 8, there is zeroth order mixing of the degenerate levels of the two H_2 molecules—A and B—forming the familiar $\sigma_{g,A} \pm \sigma_{g,B}$ and $\sigma_{u,A}^* \pm \sigma_{u,B}^*$ combinations, where $\sigma_{g,A}$ and $\sigma_{g,B}$ are the bonding molecular orbitals (MOs) of the unperturbed H_2 molecules A and B, respectively. Here, $\sigma_{u,A}^*$ and $\sigma_{u,B}^*$ are the corresponding antibonding MOs. There is no electron transfer at this conceptual stage. The resulting molecular orbitals then interact (depicted in the middle panel of Fig. 8) in a typical second-order perturbation theory manner, $\sigma_{g,A} + \sigma_{g,B}$ mixing into itself $\sigma_{u,A}^* - \sigma_{u,B}^*$, and $\sigma_{g,A} - \sigma_{g,B}$ mixing with $\sigma_{u,A}^* + \sigma_{u,B}^*$. The final result is shown at the right in Fig. 8. It is at this stage that electron transfer occurs, from σ_g to σ_u^* levels. In general, interaction implies mixing, which in turn implies delocalization along with partial electron transfer accompanying it.

3. A numerical experiment, implementing the orbital model

According to our earlier structural analysis[1] of the Pickard and Needs proposals for crystalline hydrogen in the pressure from 100 GPa to 400 GPa, the H_2 bond length increases, from 0.733 Å to 0.780 Å. Once again, we
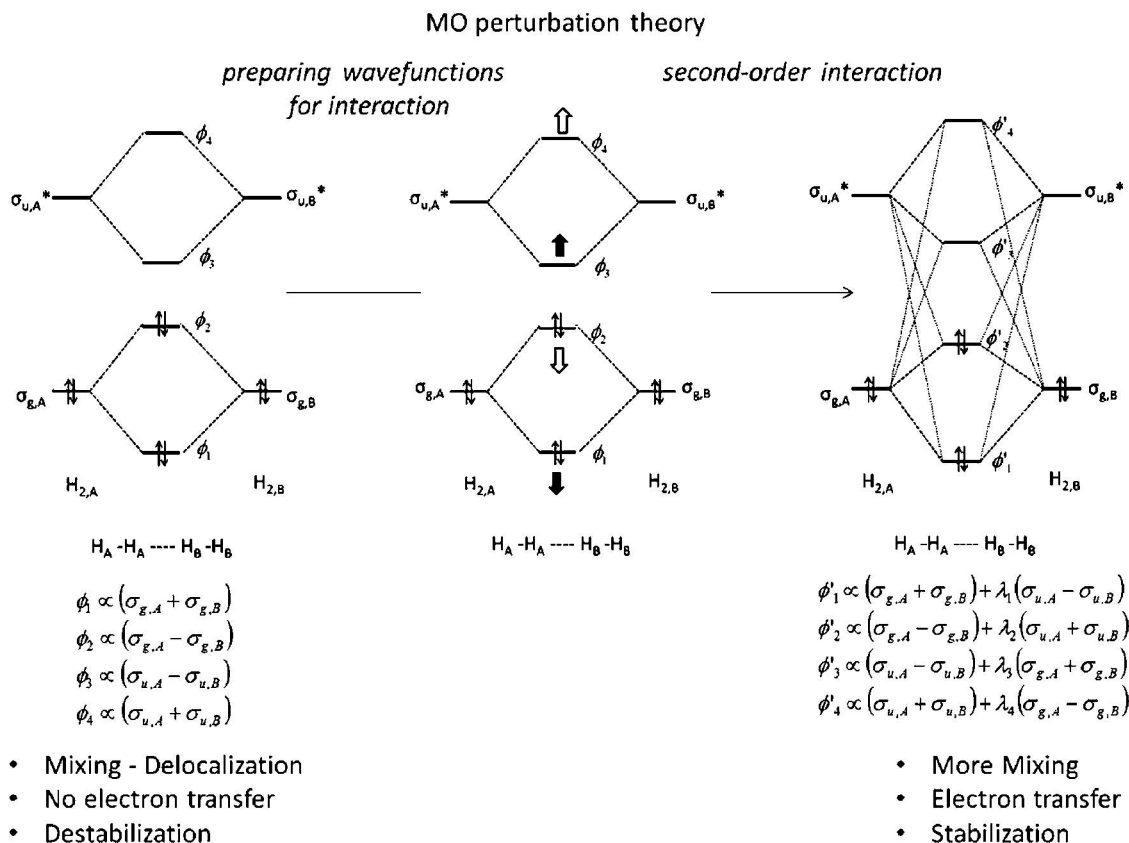
MO perturbation theory

FIG. 8. Molecular orbital diagram describing the interaction between two H_2 molecules in a linear arrangement. The perturbation is the interaction of the two molecules with each other. At left, in zeroth order of degenerate perturbation theory, the wave functions/levels are prepared for interaction by mixing σ_g of one H_2 molecule with its degenerate partner in the second molecule, and a similar mixing among the two σ_u* orbitals. In the middle and at right, second-order interactions are turned on, indicated by thin dashed lines. These effectively arise from mixing of σ_u* combinations of one H_2 with σ_g of the other H_2. The thick arrows in the middle diagram indicate the progression (in energy) of the levels as a consequence of second-order mixing.

consider a discrete molecular model, but now a ring of three H_2 molecules arranged in a D_{3h} geometry, and as sketched in Fig. 9.

This model, an arrangement of three H_2 molecules into triangles, has been chosen because in a simple way it captures a motif that is found in two of the Pickard and Needs structures for crystalline hydrogen, namely, the $C2/c$ and $Cmca$-12 structures, represented in Fig. 10, which exhibit elongated H_2 bonds.
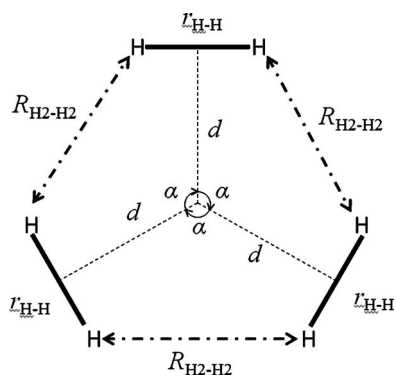
This arrangement is reminiscent of the model ring of six hydrogen atoms in the form of a regular hexagon, as first investigated by Mattheiss in 1961 (Ref. 38) and a few years later by Moskowitz.[39] It is interesting to note that in 1981, LeSar and Herschbach[40] predicted that "solid molecular hydrogen at high pressures might undergo a phase transition to form ter-molecular complexes [$(H_2)_3$] before transition to the atomic or metallic phase at still higher pressures." They did this on the basis that the regular hexagon H_6 is among the H_{4n+2} (n = 1–15) regular polygons, the only one found to be stable with respect to the dissociation of one H_2 molecule into two hydrogen atoms. Our model is also related to the study by
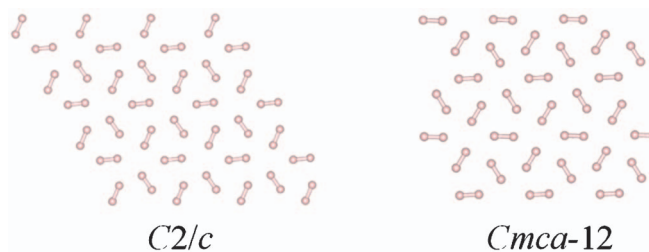

FIG. 9. D_{3h} arrangement of three H_2 molecules, also providing the definitions of d, R_{H2-H2}, and r_{H-H}.

FIG. 10. A layer of the $C2/c$, and $Cmca$-12 structures at P = 300 GPa.[2] In the $C2/c$ structure the layers are arranged in an ABCDA fashion; in the $Cmca$-12 structure they are arranged in an ABA fashion.
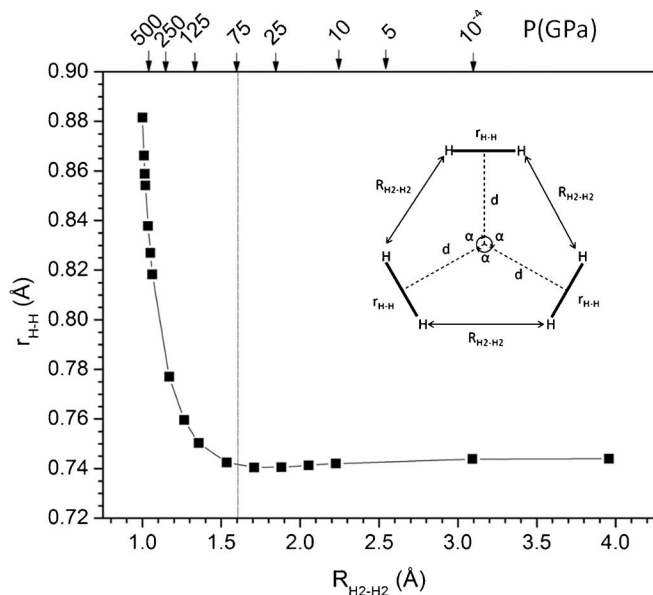
FIG. 11. Correlation between the H_2 bond length r_{H-H} and the intermolecular distance between two H_2s, R_{H2-H2}, in the D_{3h} arrangement of $3H_2$ molecules as sketched in Fig. 9. Numbers and arrows above the horizontal line at the top of the graphic are indications of the pressures required (in GPa) to observe the same intermolecular H–H separations in computations of extended structures for static hydrogen in its ground state.[1]

Ladik *et al.* on the effects of disorder on rings of hydrogen atoms.[41,42]

a. Correlation between intramolecular and intermolecular H–H distances. In this molecular model, the intramolecular H–H distance—r_{H-H}—and the shortest intermolecular H–H distance—R_{H2-H2}—were both optimized, while constraining the center of array to center of H_2 distance d. Here, our computations were performed at the DFT/B3LYP/6-311++G(d,p) level of theory. Variation of d then simulates the effect of pressure on the system. In Fig. 11 is plotted the optimal intramolecular H–H distance r_{H-H} with respect to the corresponding optimal shortest intermolecular distance between two H_2 molecules: R_{H2-H2}.

When the separation between two H_2 molecules, R_{H2-H2}, is quite large, a decrease of the intermolecular distance results in a decrease of the intramolecular H–H separation. But below a certain intermolecular separation (~1.6 Å), decreasing R_{H2-H2} actually leads in this model to an increase of the intramolecular H–H separation, in fact, exactly as is found in solid hydrogen under pressure.[1,11,12]

b. Orbital correlation diagram for three approaching H_2 molecules. This lengthening of the intramolecular H–H separation can be understood through a study of the fragment molecular orbital interactions of the three H_2 molecules. In Fig. 12 are represented the molecular orbitals of the $3H_2$-arrangement when R_{H2-H2} is chosen to be long with respect to r_{H-H}, and also when it is equal to it (symmetry D_{6h}). The molecular orbitals of D_{6h} H_6 are, of course, isomorphic to the π system of benzene. The correlation between the MOs in the two conformations is now indicated by dashed lines in Fig. 12.

At infinite separation R_{H2-H2}, the three H_2 molecules are non-interacting. The three occupied MOs can then be expressed as symmetry-adapted (D_{3h}) linear combinations of the σ_g fragment MOs of each H_2 molecule, and the three unoccupied MOs as linear combinations of the σ_u* fragment MOs of each H_2 molecule. The a_1' and $1e'$ occupied MOs are then clearly degenerate at infinite R_{H2-H2}, as are the $2e'$ and a_2'' unoccupied ones. It may also be noted that as a net result the $1e'$ levels in the σ_g block are antibonding in the intermolecular regions (repulsive interaction), whereas the $2e'$ levels in the σ_u* block are bonding (attractive interaction). At large intermolecular H–H separation, overlap between orbitals of each H_2 fragment is so small that this antibonding/bonding character in the intermolecular regions has no effect on the energy levels. But as the distance R_{H2-H2} decreases, interaction in the σ_g manifold now places a_1' below $1e'$, and in the σ_u* block $2e'$ below a_2''.

The repulsive interaction in the σ_g block, which would elevate the $1e'$ (constructed from the σ_g of H_2) orbitals high in energy in zeroth order of perturbation theory, is mitigated by a mixing of $1e'$ with $2e'$ (constructed from the σ_u* of H_2), stabilizing the former. The net result is a partial occupation of the σ_u* fragment MOs of each H_2 molecule and a partial depopulation of the σ_g fragment MOs, concomitant with a decrease of the antibonding character or increase of the bonding character in the intermolecular regions. The extent of this mixing increases with the decrease of the R_{H2-H2} intermolecular distance. Accordingly, orbital interactions both weaken the intramolecular H–H interaction and strengthen the intermolecular one. To put it in other words, orbital interactions weaken existing bonds but in the process create new bonds in the intermolecular regions.

Certainly, as the degree of equalization of R_{H2-H2} and r_{H-H} increases (modeling an increase in pressure), the coordination number of the H atoms rises. The system can be thought as having two Kékulé structures, as in benzene.[43] When R_{H2-H2} becomes perfectly equal to r_{H-H}, the system is of D_{6h} symmetry. There are then no discrete H_2 molecules; the six hydrogens are entirely equivalent. Choosing one of the two equivalent definitions for H_2 molecular fragments, and thinking of the σ_g and σ_u* MOs of these fragments, then results in population of the σ_u* fragment MOs (and equal depopulation of σ_g) by 1/3 of an electron. Note that an actual optimization of the H–H distance in the D_{6h} symmetry, without further constraint, leads to an H–H separation of 0.992 Å.

Although the intramolecular and intermolecular H–H separations become equalized (in this model, and also in the structures of hydrogen under pressure that it models), the σ_u* fragment MO population remains far below 1. From this point of view, if the H_2 molecules can be thought of as dissociated, the H–H covalent bonds are not; they are simply weakened (and non-bonded H–H interactions are correspondingly strengthened). There is still H–H bonding, but perhaps one can view this bonding as one-electron two-center, with H_2^+ ($r_{H-H} = 1.052$ Å) as a model. Or one can also think of each of the H_2 molecules as "partially excited," σ_g electrons shifted to σ_u*.

c. Intramolecular and intermolecular bond indices. The weakening of the intramolecular H–H bonds as the intermolecular separations decrease is a natural consequence of
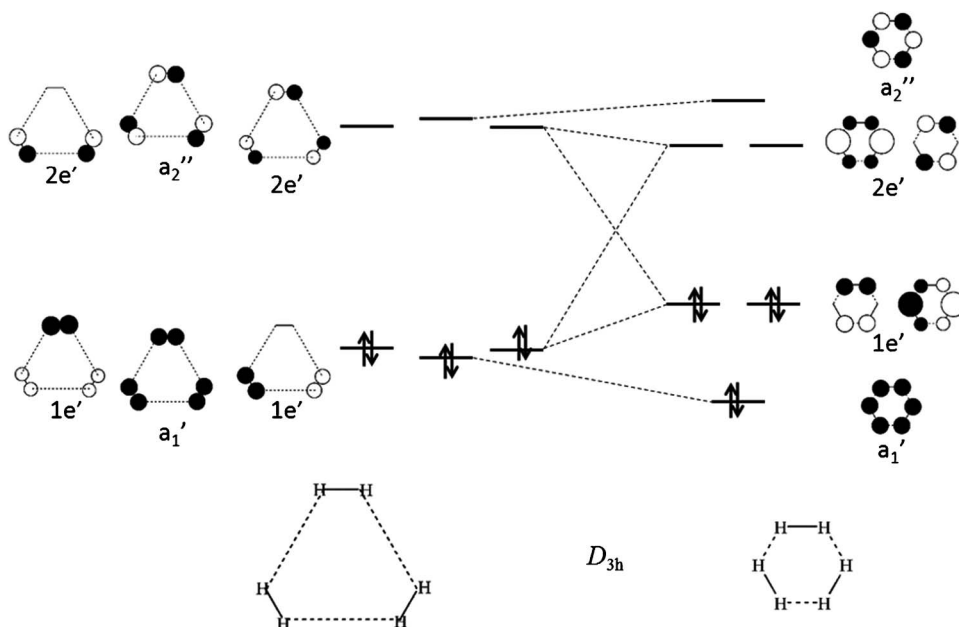
FIG. 12. Correlation diagram between the molecular orbitals (MOs) of $3H_2$ in a D_{3h} configuration when the intermolecular H–H distance is large with respect to the intramolecular counterpart (left) and when it is of the same order, and actually identical (right). Each molecular orbital is labeled in the D_{3h} point group of symmetry. Black and white again indicate phases of the wave function. See text for an explanation of the orbital drawings.

the induced electronic redistribution which, under the constraint of conserving the total number of electrons, tends to strengthen the intermolecular H–H interactions. One way to see this is to follow the evolution of intramolecular and intermolecular bond indices as the degree of equalization of the intramolecular and shortest intermolecular H–H separations increases.

Several bond order indices, correlated with bond strength, have been developed in quantum chemistry since the late 1930s. Oldest among these is the Mulliken overlap population (MOP) (Ref. 44) between a pair of atoms A–B. Other popular indices are the Wiberg[45] (WBO) and the Mayer (MBO) (Refs. 46–49) bond order indices. Their definitions are now given.

In the linear combination of atomic orbitals approximation, the wave function for an N-electron molecular system can be expressed as a Slater determinant constructed from N molecular spin-orbitals. The space part of these molecular spin-orbitals—the molecular orbitals—can in turn be expressed using a basis of atomic functions, i.e., as linear combinations of atomic orbitals:

$$\phi_i (\vec{r}) = \sum_{\mu=1}^{N_{\text{basis}}} c_{i\mu} \chi_\mu (\vec{r})$$

with ϕ_i being the ith molecular orbital, χ_μ being the μth atomic orbital in a basis of atomic function of dimension N_{basis}, and $c_{i\mu}$ being the coefficient of χ_μ in ϕ_i.

The density matrix (D) and overlap matrix (S) elements are then defined, respectively, as

$$D_{\mu\nu} = \sum_{i=1}^{N_{\text{basis}}} n_i c_{i\mu} c_{i\nu}^*$$

with n_i being the occupation of the ith molecular orbital ϕ_i, and for the overlap matrix

$$S_{\mu\nu} = \int \chi_\mu (\vec{r}) \chi_\nu^* (\vec{r}) \, d\vec{r}.$$

In this framework, the WBO, MBO, and MOP between a pair of atoms A–B are defined, respectively, as

$$\text{WBO}_{AB} = \sum_{\mu \in A} \sum_{\nu \in B} (D_{\mu\nu})^2,$$

$$\text{MBO}_{AB} = \sum_{\mu \in A} \sum_{\nu \in B} (DS)_{\mu\nu} (DS)_{\nu\mu},$$

and

$$\text{MOP}_{AB} = \sum_{\mu \in A} \sum_{\nu \in B} D_{\mu\nu} S_{\mu\nu}.$$

By definition the WBO takes on positive values only, while the MBO and the MOP can be negative. Note that with this definition, the WBO has to be computed within an orthogonal basis. We have computed it in the NBO basis.[50]

Figure 13 shows the evolution of the three bond order indices in the D_{3h}-$3H_2$ model as d decreases, both for intramolecular (Fig. 13(a)) and intermolecular (Fig. 13(b)) H–H pairs.

The three indices can be seen to follow the same trend as the intermolecular H–H separation decreases in the system; they decrease between those Hs that are paired at long intermolecular H–H separations and increase between those which belong to neighboring H_2 molecules. The intramolecular Mulliken overlap population is not constrained to give a value of 1.0 for a full bond (in that sense, it cannot be considered as a bond order index), and so begins with a different value at large intermolecular separations, eventually joining the other indices. On the other hand, the WBO and the MBO indices are
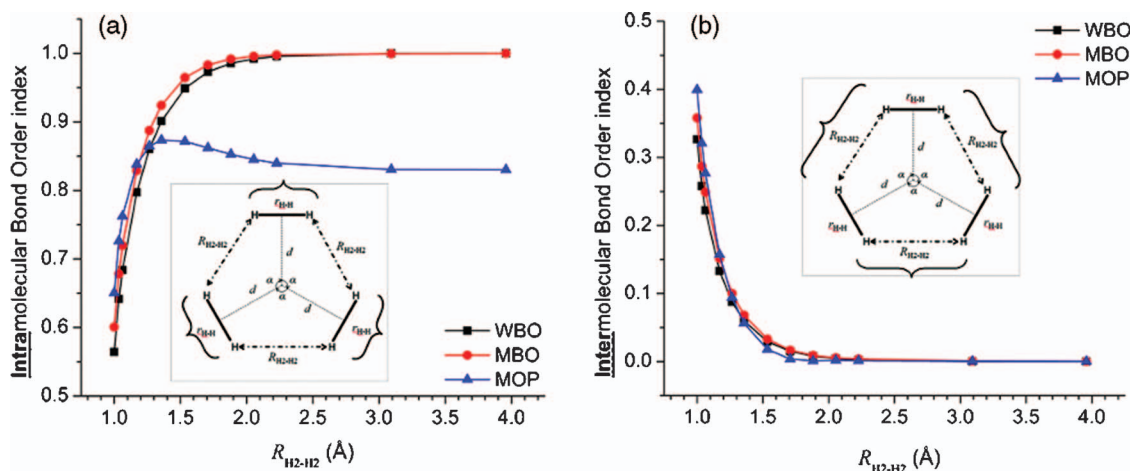
FIG. 13. Wiberg bond order index (WBO), Mayer bond order index (MBO), and Mulliken overlap population (MOP) between some H–H pairs of the D_{3h}-3H$_2$ arrangement. The H–H pairs considered are indicated by the curly brackets: (a) intramolecular and (b) intermolecular.

very close to each other, taking on values between 1 and 0.5 for the intramolecular pairs, and between 0 and 0.5 for the intermolecular pairs, in agreement with our previous analysis of the orbital correlation diagram (see Fig. 12). The three indices also give the same picture of the evolution of intramolecular and intermolecular H–H bonding: strengthening of the H–H intermolecular bonds because of increased overlap between orbitals of neighboring molecules actually induces weakening of the intramolecular H–H bonds.

Our numerical experiment is a good illustration of the fact that there is no dichotomy between the presence and absence of a "chemical bond." In chemical reactions as well as in numerical experiments, at normal pressure or as the pressure is increased greatly, bonds evolve, and they are made or they break in a continuous way.

A natural next step would be to examine to what extent the arguments just developed in the case of a discrete molecular system hold when many such discrete arrays (of molecules) are brought close to each other, as in dense hydrogen under an increase of pressure. This is what we will see in the next paper of this series,[51] where we will study the evolution of the σ_g and σ_u^* orbitals of the H$_2$ units in the candidate extended structures for dense hydrogen.

IV. SUMMARIZING: A PHYSICAL EFFECT AND A CHEMICAL EFFECT

In this paper we have presented two models for the progression of the intramolecular H–H separation as neighboring H$_2$ molecules are induced to become closer and closer, this being a natural consequence of an increase of pressure. Simple confinement of H$_2$, simulated by a plausible model already in the literature, or by squeezing two hydrogens between He atoms, results as density increases only in a diminution of the H$_2$ bond length, and a corresponding rise in force constant for the vibron.

A "chemical" effect, which could just as well be called an orbital effect of interaction of H$_2$ molecules, is an increase in the population upon compression of H$_2$ σ_u^* orbitals and a depopulation of σ_g orbitals. These actions elongate the bond,

as we have shown with a numerical experiment. As we will see in the third paper in this series,[51] the two effects, actually competing with each other, are likely to be responsible for the small "dance" that takes place in the H–H separation as hydrogen is compressed.

[1]V. Labet, P. Gonzalez-Morelos, R. Hoffmann, and N. W. Ashcroft, J. Chem. Phys. **136**, 074501 (2012).
[2]C. J. Pickard and R. J. Needs, Nat. Phys. **3**, 473 (2007).
[3]R. M. Badger, J. Chem. Phys. **2**, 128 (1934).
[4]D. R. Herschbach and V. W. Laurie, J. Chem. Phys. **35**, 458 (1961).
[5]A. B. Anderson and R. G. Parr, Chem. Phys. Lett **10**, 293 (1971).
[6]C$_2$ is an example, O. G. Landsverk, Phys. Rev. **56**, 769 (1939); R. S. Mulliken, *ibid.* **56**, 778 (1939); K. P. Huber and G. Herzberg, *Molecular Spectra and Molecular Structure. IV. Constants of diatomic molecules* (Van Nostrand Reinhold, New York, 1979).
[7]J. Van Kranendonk, Physica **23**, 825 (1957).
[8]J. Van Kranendonk, Physica **25**, 1080 (1959).
[9]J. Van Kranendonk, Can. J. Phys. **38**, 240 (1960).
[10]J. Van Kranendonk, *Solid Hydrogen* (Plenum, New York, 1983).
[11]P. Loubeyre, M. Jean-Louis, and I. F. Silvera, Phys. Rev. B **43**, 10191 (1991).
[12]F. Grazzi, M. Moraldi, and L. Ulivi, Europhys. Lett. **68**, 664 (2004).
[13]I. F. Silvera and R. J. Wijngaarden, Phys. Rev. Lett. **47**, 39 (1981).
[14]S. K. Sharma, H. K. Mao, and P. M. Bell, Phys. Rev. Lett. **44**, 886 (1980).
[15]S. K. Sharma, H. K. Mao, and P. M. Bell, Phys. Rev. Lett. **46**, 1109 (1981).
[16]M. J. Frisch, G. W. Trucks, H. B. Schlegel, *et al.*, GAUSSIAN 03, Revision B.04, Gaussian, Inc., Pittsburgh, PA, 2003.

[17] C. Møller and M. S. Plesset, Phys. Rev. **46**, 618 (1934).

[18] M. Head-Gordon, J. A. Pople, and M. J. Frisch, Chem. Phys. Lett. **153**, 503 (1988).

[19] S. Saebø and J. Almlöf, Chem. Phys. Lett. **154**, 83 (1989).

[20] M. J. Frisch, M. Head-Gordon, and J. A. Pople, Chem. Phys. Lett. **166**, 275 (1990).

[21] M. J. Frisch, M. Head-Gordon, and J. A. Pople, Chem. Phys. Lett. **166**, 281 (1990).

[22] R. G. Parr and W. Yang, *Density-Functional Theory for Atoms and Molecules* (Oxford University Press, New York, 1989), and references therein.

[23] C. Lee, W. Yang, and R. G. Parr, Phys. Rev. B **37**, 785 (1988).

[24] B. Miehlich, A. Savin, H. Stoll, and H. Preuss, Chem. Phys. Lett. **157**, 200 (1989).

[25] A. D. Becke, J. Chem. Phys. **98**, 5648 (1993).

[26] J. P. Foster and F. Weinhold, J. Am. Chem. Soc. **102**, 7211 (1980).

[27] R. LeSar and D. R. Herschbach, J. Phys. Chem. **85**, 2798 (1981).

[28] H. M. James and A. S. Coolidge, J. Chem. Phys. **1**, 825 (1933).

[29] G. J. Kubas, J. Organomet. Chem **635**, 37 (2001).

[30] G. J. Kubas, Chem. Rev. **107**, 4152 (2007).

[31] F. Maseras, A Lledos, E. Clot, and O. Eisenstein, Chem. Rev. **100**, 601 (2000).

[32] G. J. Kubas, R. R. Ryan, B. I. Swanson, P. J. Vergamini, and H. J. Wasserman, J. Am. Chem. Soc. **106**, 451 (1984).

[33] J.-Y. Saillard and R. Hoffmann, J. Am. Chem. Soc. **106**, 2006 (1984).

[34] S. L. Mattews, V. Pons, and D. M. Heinekey, J. Am. Chem. Soc. **127**, 850 (2005).

[35] L. Brammer, J. A. K. Howard, O. Johnson, T. F. Koetzle, J. L. Spencer, and A. M. Stringer, J. Chem. Soc., Chem. Commun. **1991**, 241.

[36] K. A. Johnson and N. W. Ashcroft, Nature (London) **403**, 632 (2000).

[37] See, however, the recent claim for hydrogen metallization at ∼270 GPa and 30–295 K: M. I. Eremets and I. A. Troyan, Nature Mater. **10**, 927 (2011).

[38] L. F. Mattheiss, Phys. Rev. **123**, 1209 (1961).

[39] J. W. Moskowitz, J. Chem. Phys. **38**, 677 (1963).

[40] R. LeSar and D. R. Herschbach, J. Phys. Chem. **85**, 3787 (1981).

[41] R. Day, J. Ladik, and F. Martino, Chem. Phys. Lett. **81**, 494 (1981).

[42] C.-M. Liegener and J. Ladik, Phys. Lett. A **107**, 79 (1985).

[43] Because the mass of the hydrogen atoms is small, a legitimate question to ask in a real system of three hydrogen molecules is whether the exchange process might involve proton tunneling. Our interest here is, however, just in the bond forming and breaking processes.

[44] R. S. Mulliken, J. Chem. Phys. **23**, 1833, 1841, 2338, 2343 (1955).

[45] K. B. Wiberg, Tetrahedron **24**, 1083 (1968).

[46] I. Mayer, Chem. Phys. Lett. **97**, 270 (1983).

[47] I. Mayer, Chem. Phys. Lett. **117**, 396 (1985).

[48] I. Mayer, Int. J. Quantum Chem. **29**, 73 (1986).

[49] I. Mayer, Int. J. Quantum Chem. **29**, 477 (1986).

[50] A. E. Reed, R. B. Weinstock, and F. Weinhold, J. Chem. Phys. **83**, 735 (1975).

[51] V. Labet, R. Hoffmann, and N. W. Ashcroft, J. Chem. Phys. **136**, 074503 (2012).